Japanese Journal of Applied Physics **52** (2013) 10MD01 **REGULAR PAPER**
http://dx.doi.org/**10.7567/JJAP.52.10MD01**

Enhanced Gas Sensing Characteristics of Ag_2O-Functionalized Networked In_2O_3 Nanowires

Hyoun Woo Kim*, Han Gil Na, Dong Sub Kwak, Hong Yeon Cho, and Yong Jung Kwon

Division of Materials Science and Engineering, Hanyang University, Seoul 133-791, Korea
E-mail: hyounwoo@hanyang.ac.kr

Received November 23, 2012; accepted June 20, 2013; published online October 21, 2013

We have fabricated Ag_2O-functionalized In_2O_3 nanowires, in which the NO_2 gas sensing properties are enhanced. To achieve the functionalization, the core In_2O_3 nanowires were sputter-deposited with the Ag shell layer, which turned out to be composed of cubic Ag particles. Subsequent thermal annealing changed the Ag nanoparticles to cubic nanoparticles with a cubic Ag_2O phase. In spite of shell-coating and subsequent annealing, scanning electron microscopy images revealed that the products consisted of one-dimensional nanowires. In a NO_2 gas sensing test, the sensitivity of the Ag_2O-functionalized sensor was lower than that of the nonfunctionalized sensor, presumably owing to the significant volume of the depletion region in the Ag_2O–In_2O_3 interface. However, the Ag_2O-functionalized In_2O_3 nanowires exhibited exceptionally fast response and recovery compared with bare In_2O_3 nanowires. We suggest that not only the catalytic effect but also the spillover effect of Ag_2O nanoparticles is mainly responsible for the observed enhancement of sensing capabilities in terms of response/recovery time.

1. Introduction

Indium oxide (In_2O_3) is a promising material for sensing gases such as O_2,[1] O_3,[2,3] nitric oxides,[4] CO,[5,6] and H_2.[5,6] In particular, the band gap of In_2O_3 has been estimated to be 2.9 eV. It is much narrower than those of other metal oxides such as WO_3, SnO_2, and ZnO, making In_2O_3 suitable for low-temperature gas sensing.[7] To further enhance the sensor characteristics, we have adopted two strategies: the use of networked nanowire structures and nanoparticle catalysts.

First, because their one-dimensional (1D) nanostructures exhibit specific physical and chemical properties,[8–13] metal oxide semiconductor nanowires have excellent gas sensitivity, owing to their exceptionally high surface-to-volume ratio, semiconducting electrical behavior, and single-crystalline assembly.[14,15] In order to obtain reliable gas sensors while avoiding the expensive photolithography process, expensive measuring system, and large variation in measured current values, in the case of using single nanowires, we have employed networked multiple nanowires.[16]

Second, catalysts, in the form of particles or dopants, are known to functionalize the surface of nanomaterials, whereby catalysts anchored on semiconducting oxides enhance the sensing characteristics by facilitating the dissociation of adsorbed species. Up to now, a variety of materials, including Pd thin layers,[17] Pt nanoparticles,[18] Pd/PdO nanoparticles,[19] CuO islands,[20] Pd/Pt alloy films,[21] and Co–Ce oxide films,[22] have been studied for their use as sensor catalysts. The catalysts are considered to enhance the sensing characteristics via a variety of mechanisms. It is possible that metal ions form a solid solution, changing the adsorption and gas sensing properties.[23] Metal atoms are dissolved within the lattice, producing localized gap states, and eventually enhancing tunneling currents through the surface barriers.[24] Also, catalysts can induce spillover effects, enhancing not only the adsorption of the gas species but also the diffusion of those species onto the sensor surface.

Nitrogen dioxide (NO_2) is one of the most toxic components that causes the serious problem of atmospheric air pollution and thereby has adverse effects on the human respiratory system.[25] It is one of the most harmful gases, being emitted from automobile exhaust, home heaters, furnaces, and plants, for example. Accordingly, it is urgent to develop sensors with sufficient sensitivity and quicker response time to detect NO_2 at low concentrations, such as 3 to 4 ppm.[26] Since it has been demonstrated that In_2O_3 thin-film sensors are sensitive to low concentrations of NO_2 gas in air,[3,23,27–29] it is most urgent to achieve fast response and recovery, especially at low concentrations, in order to prevent fatal damage to the human respiratory system. Additionally, fast response and recovery will reduce the power consumption of the sensor.

In the present study, in order to attain short response and recovery times with an acceptable sensitivity at a low concentration of NO_2, we have prepared Ag_2O-functionalized and networked In_2O_3 nanowires. To the best of our knowledge, this is the first report on Ag_2O-functionalized In_2O_3 nanowires. By thermal annealing, we fabricated Ag_2O-phased nanoparticles on the surface of In_2O_3 core nanowires. We then compared the NO_2 gas sensing characteristics of Ag_2O-functionalized In_2O_3 nanowires with those of bare nanowires.

2. Experimental Procedure

In the present process, the In_2O_3 core nanowires were synthesized using a tube furnace, which was previously outlined.[30] A mixture of In and Mg nanopowders was used as an evaporation source (weight ratio of 1 : 1). The fabrication procedure of In_2O_3 nanowires is analogous to that in the previous work.[18] The substrate temperature was set to 800 °C for 1 h, with a flow of a mixture of Ar and O_2 gases (O_2 partial pressure: 3%). Subsequently, we coated the Ag shell using a turbo-sputter coater (Emitech K575X).[22] During the sputtering process with the DC current of 10 mA, we carried out sputter deposition with a circular Ag target at room temperature in high-purity (99.999%) argon (Ar) ambient. Subsequently, the In_2O_3-core/Ag-shell nanowires were heated at 500 °C for 30 min in Ar ambient.

The products were characterized by X-ray diffraction (XRD; Philips X'pert MRD) and field emission scanning electron microscopy (FE-SEM; Hitachi S-4200). We acquired transmission electron microscopy (TEM) images, selected-area electron diffraction (SAED) patterns, and

energy-dispersive X-ray (EDX) spectra using a Philips CM-200 TEM system operated at 200 kV, which was installed at KBSI.

In order to measure the sensing properties of NO_2 gas, double-layer electrodes (200-nm-thick Ni/50-nm-thick Au) were sequentially sputtered onto the specimens with an interdigital electrode mask. The fabricated sensors were introduced into a vacuum chamber (base pressure: $\sim 5 \times 10^{-6}$ Torr) and their electrical conductivity was measured at different NO_2 concentrations at 250 °C. A similar experimental setup was previously used.[31–34] The sensitivity (S) was determined via the following formula: $S = R_{NO2}/R_{air}$, where R_{air} and R_{NO2} are resistances in air ambient and in the presence of NO_2 gas, respectively. The response and recovery times were defined as the time taken to reach a 90% change in the resistance upon the supply or removal of the target gas, respectively.[35]

3. Results and Discussion

Figure 1(a) shows the XRD pattern of bare In_2O_3 nanowires, in which most diffraction peaks correspond to the cubic In_2O_3 phase (JCPDS No. 06-0416), although there exist very weak diffraction peaks corresponding to the (111) and (311) reflections of the cubic Au phase, with lattice constants of $a = 4.0786$ Å (JCPDS No. 04-0784). Figures 1(b) and 1(c) show the XRD patterns before and after thermal annealing at 500 °C, respectively. Similarly to the case of the bare In_2O_3 nanowires, both patterns mainly exhibit the reflection peaks corresponding to the cubic In_2O_3 phase. In the case of Ag-coated In_2O_3 nanowires without subsequent annealing [Fig. 1(b)], there exist very weak peaks that correspond to the (111) reflection of cubic Au/cubic Ag [$a = 4.0862$ Å (JCPDS No. 04-0783)] and to the (200) reflection of cubic Au/cubic Ag. Since cubic Au and Ag phases are overlapped on those peaks, it is not clear that these reflections indeed originate from the cubic Ag structure. In the case of Ag-coated In_2O_3 nanowires, which were subsequently annealed at 500 °C [Fig. 1(c)], we observe the very weak peaks corresponding to (200), (220), and (311) reflections of the cubic Ag_2O phase with the lattice constant of $a = 4.7263$ Å (JCPDS No. 41-1104).

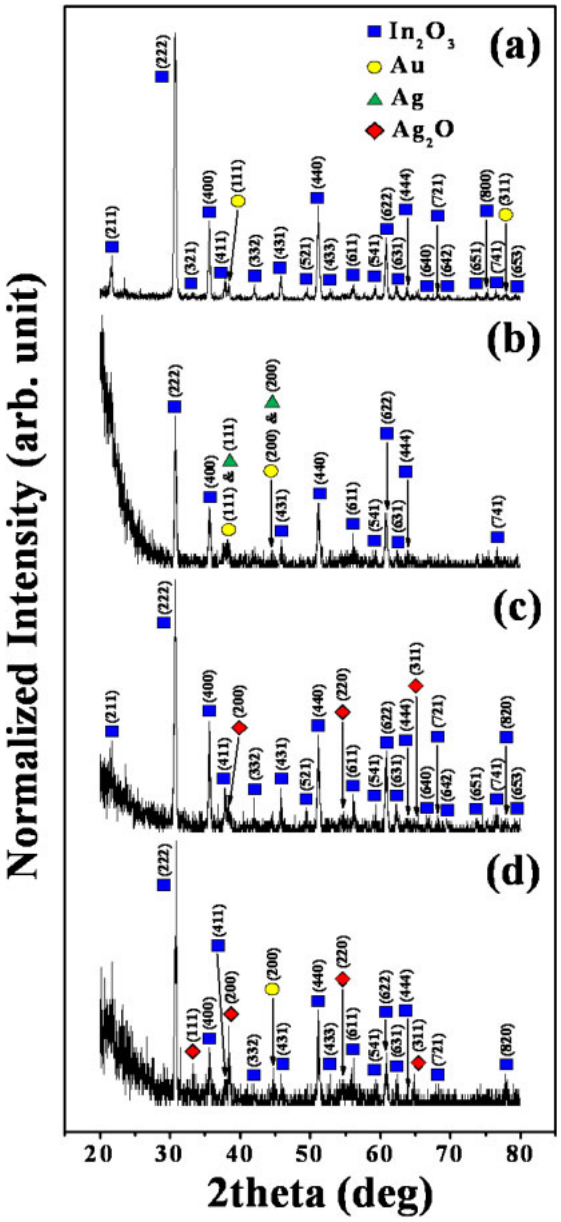

Fig. 1. (Color online) XRD patterns of (a) as-fabricated In_2O_3 core nanowires, and Ag-coated core-shell nanowires (b) before and (c) after thermal annealing at 500 °C.

Figure 2(a) shows a SEM image of the bare In_2O_3 nanowires, whereas Figs. 2(b) and 2(c) show the SEM images of Ag-coated In_2O_3 nanowires without and with annealing, respectively. It is observed that the products are composed of 1D structures, regardless of the Ag shell coating or subsequent annealing. The right-hand-side images in Fig. 2 are the enlarged SEM images. Although the bare In_2O_3 nanowire exhibits a relatively smooth surface, the Ag-coated In_2O_3 nanowires show a rough surface.

In order to investigate the structure and morphology of nanowires in more detail, we carried out the TEM analyses. Figure 3(a) shows a low-magnification TEM image of a bare In_2O_3 nanowire, indicating that nanoparticle-like structures reside on the surface. Figures 3(b) and 3(c) show the TEM–EDX spectra of the regions without and with nanoparticles, respectively. By comparing Fig. 3(c) with Fig. 3(a), we find that the nanoparticles exhibit the Ag-related peak, in addition to the Co, Cu, In, and O peaks, as observed in the core In_2O_3 region. In this case, it is evident that Cu and C signals are associated with the carbon-coated Cu grid that supports the nanowire. Accordingly, we surmise that the nanoparticle-like structures comprise Ag elements. The SAED pattern taken from the nanoparticle-containing region is shown in Fig. 3(d). The regularly positioned diffraction spots were indexed as cubic In_2O_3, including (020), (200), and (220) reflections. In addition, diffraction ring spots corresponding to the (111) and (200) lattice planes of cubic Ag (JCPDS No. 04-0783) were clearly observed. The spotty pattern of In_2O_3 reveals a single crystal nature, whereas Ag ring spots correspond to a polycrystalline nature. Figure 3(e) shows a lattice-resolved TEM image taken from the interface between the In_2O_3 core and Ag nanoparticle. The measured lattice spacing in the core region is 0.25 nm, which corresponds well with the d-value of the {400} plane of cubic In_2O_3. The lattice spacing measured from the Ag lattice image is 0.24 nm, corresponding well to the d-value of the (111) plane of cubic Ag.

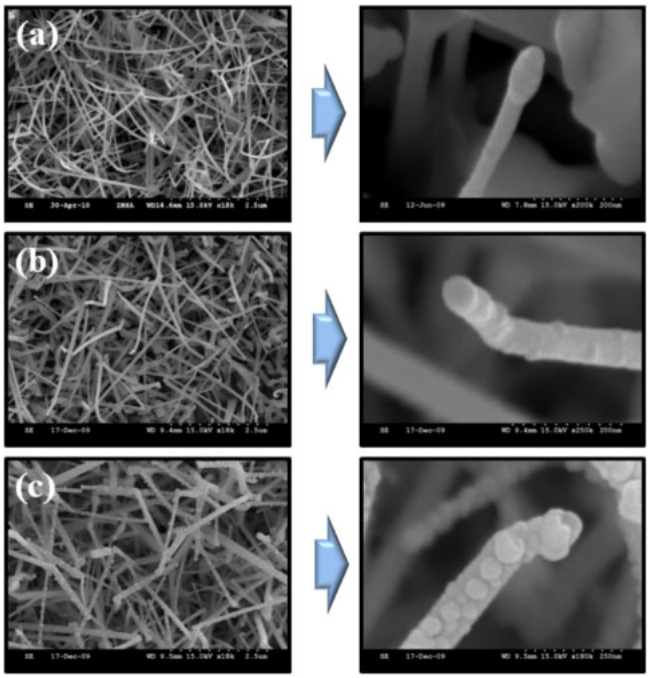

Fig. 2. (Color online) SEM images of (a) as-fabricated In_2O_3 core nanowires, and Ag-coated core-shell nanowires (b) before and (c) after thermal annealing at 500 °C. Right-hand-side images correspond to the enlarged SEM images.

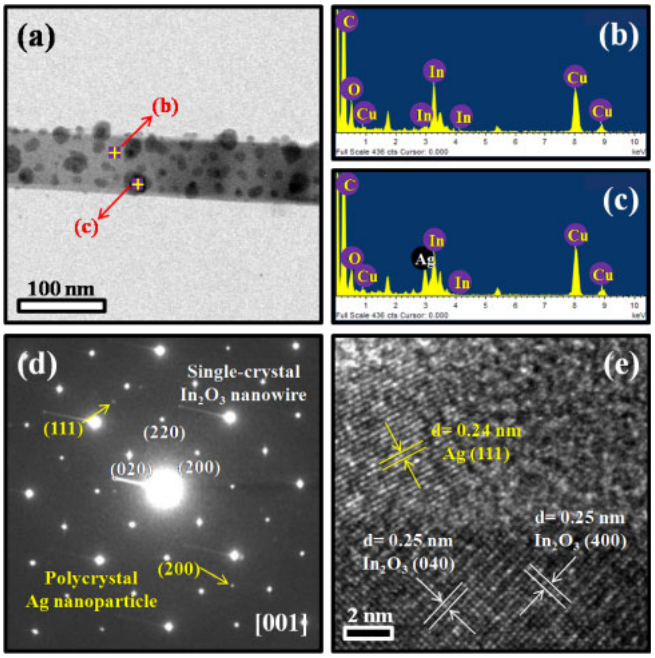

Fig. 3. (Color online) (a) Low-magnification TEM image of an as-fabricated In_2O_3 core nanowire. EDX spectra of the (b) core and (c) nanoparticle regions indicated in (a). (d) SAED pattern and (e) lattice-resolved TEM image of enlarged area including the interface between In_2O_3 core and nanoparticle.

Figure 4(a) shows a low-magnification TEM image of a 500 °C-annealed In_2O_3/Ag core–shell nanowire. The 1D structure exhibits a rough surface consisting of various nanoparticles. Figure 4(b) is a lattice-resolved TEM image, in which the nanowire image consists of bright (In_2O_3 core)

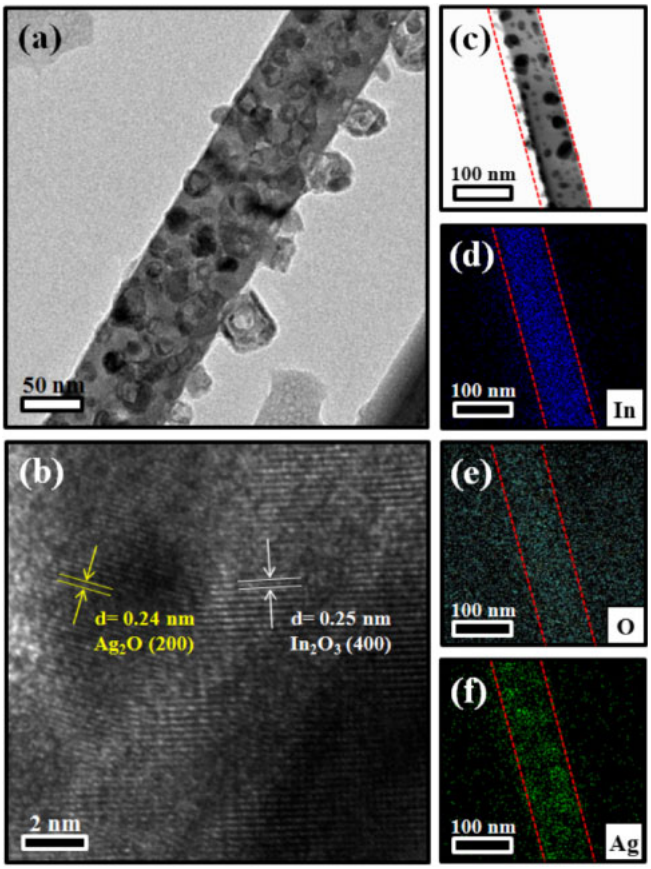

Fig. 4. (Color online) (a) Low-magnification TEM image of as-fabricated In_2O_3 core nanowire. (b) Lattice-resolved TEM image, showing the In_2O_3 core and nanoparticles. (c) TEM image of a typical nanowire, and EDX elemental maps of (d) In, (e) O, and (f) Ag elements.

and dark (nanoparticle) regions. The lattice spacings in core and nanoparticle regions, respectively, match the (400) plane of cubic In_2O_3 and the (200) plane of cubic Ag_2O. Figure 4(c) shows a single nanowire and Figs. 4(d)–4(f) are the corresponding elemental maps of In, O, and Ag elements, respectively, obtained by the TEM–EDX technique. It is revealed that In and O elements are uniformly distributed on the surface of the nanowire, whereas the distribution of Ag elements coincides well with the Ag nanoparticles in Fig. 4(c).

To assess the potential applicability of the gas sensors based on In_2O_3 nanowires with or without Ag_2O functionalization, we compared their sensing properties with respect to NO_2 gas. Figures 5(a) and 5(b) show typical response curves to NO_2 gas at 250 °C for sensors fabricated from the pure and functionalized In_2O_3 nanowires, respectively. Both curves show three sensing cycles with the introduction of 2, 6, and 10 ppm of NO_2 gas. We obtained good repeated testing cycles in all cases.

As shown in Fig. 5, the resistance increases upon exposure to NO_2, whereas it decreases upon exposure to air, which is explainable in the framework of a normal n-type semiconductor sensor. Although numerous researchers have suggested sensing mechanisms, all of them included the adsorption of NO_2 gas to the In_2O_3 surface and the subsequent extraction of electrons. The absorbed NO_2 extracts electrons from the conduction band of the n-type

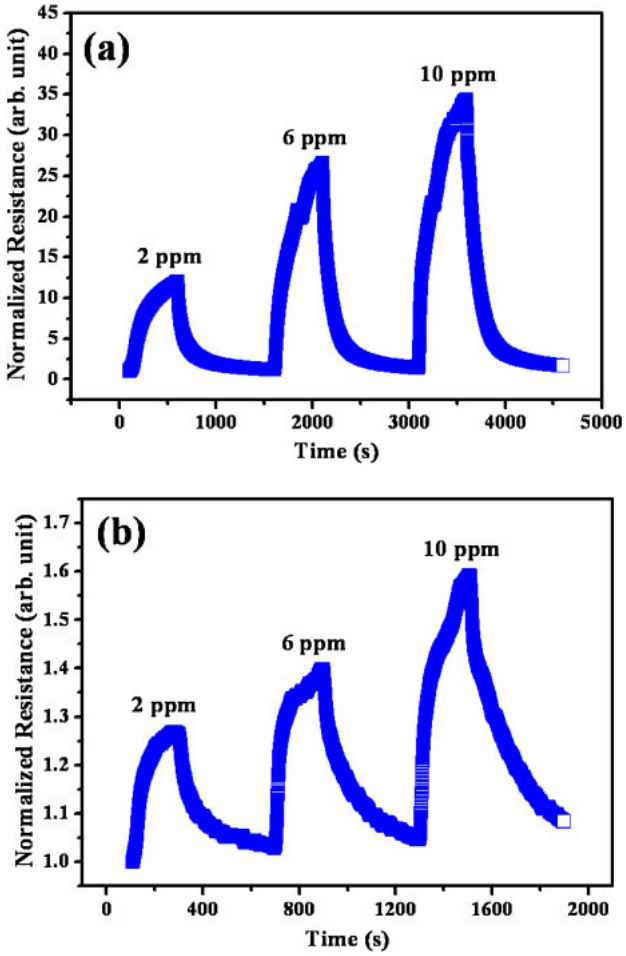

Fig. 5. (Color online) Typical dynamic response curve for various concentrations of NO_2 gas in a sensor fabricated from (a) as-fabricated In_2O_3 core nanowires and (b) 500 °C-annealed In_2O_3/Ag core-shell nanowire.

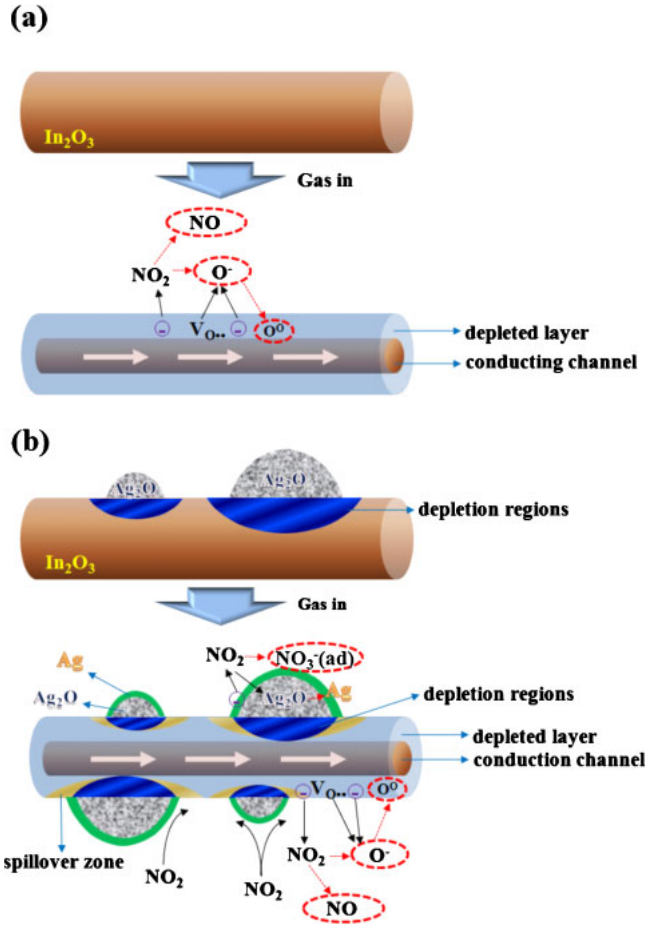

Fig. 6. (Color online) Schematics explaining the changes in the NO_2 sensing behavior (a) without and (b) with Ag_2O functionalization.

In_2O_3 nanowires and thus reduces the electron concentration near the surface. The relevant reactions include $NO_2 + e^- \rightarrow NO + O^-$.[36] In addition, dissociated O^- reacts with oxygen vacancies in the In_2O_3 surface, and extracts electrons by the following reaction: $O^- + V_O{}^{2+} + e^- \rightarrow O^O$. The deficiency of electrons increases the width of the electron depletion layers, resulting in the increased resistance of the sensors. On the other hand, the release of electrons occurs during the complicated reverse reactions, ultimately generating NO_2 gas. Subsequently, the produced NO_2 gas will desorb from the In_2O_3 surface.

In the presence of Ag_2O nanoparticles on the In_2O_3 surface, however, the role of Ag_2O as well as In_2O_3 must be sufficiently elucidated. In_2O_3 is an n-type semiconductor, whereas Ag_2O is a p-type semiconductor. Since the work function of Ag_2O (5.3 eV) is larger than that of n-type In_2O_3 (5.0 eV), the depletion layer will be formed at the interface in In_2O_3.[37] Also, the Ag_2O nanoparticles separately reside on the In_2O_3 surface, each particle being electrically isolated. Accordingly, the main electric carrier in the present In_2O_3/Ag_2O composite system is an electron, as in the case of the pure In_2O_3 system. Therefore, it is hypothesized that the conduction channel in the nanowire should be significantly reduced when there is a nonconductive depletion region.

When NO_2 gas is introduced into the system, NO_2 will be absorbed on the exposed In_2O_3 surface. By reactions analogous to those mentioned above, electrons will be extracted from In_2O_3, increasing the resistance of the sensors. Some NO_2 molecules will also adsorb on the Ag_2O surface. When the Ag_2O surface is exposed to a reducing gas, such as ethanol, Ag_2O can be reduced efficiently to Ag.[37] Even when using an oxidizing gas such as NO_2, Ag_2O can be reduced by the following reaction: $NO_2 + Ag_2O + e^- \rightarrow NO_3{}^-(ad) + 2Ag$.[38] In the present case of using oxidizing gas, however, it is unlikely that Ag_2O is completely reduced to Ag. Since the outmost surface of Ag_2O nanoparticles attached to In_2O_3 core particles can be converted to Ag under appropriate process conditions,[39] we surmise that the outer surface of the Ag_2O nanoparticles has been converted to Ag, during exposure to flowing NO_2 gas.

Figures 6(a) and 6(b) show schematics outlining the changes in the NO_2 sensing behavior without and with Ag_2O functionalization, respectively. Upon comparing Figs. 6(b) with 6(a), we understand that the conducting channel of the In_2O_3 core, in the initial stage without introducing NO_2 gas, is significantly decreased by the Ag_2O functionalization, presumably owing to the large depletion volume caused by the presence of the In_2O_3 core/Ag_2O interface. On the other hand, from our experiences, the volume of the conducting channel becomes negligibly small upon exposure to flowing NO_2 gas, in both cases of with and

Table I. Variations of response time, recovery time, and sensitivity at various NO_2 concentrations for NO_2 sensing without and with Ag_2O functionalization.

	NO_2 concentration (ppm)	Response time (s)	Recovery time (s)	Sensitivity
Normal In_2O_3 nanowires	2	345.12	286.33	12.06
	6	340.27	240.58	21.76
	10	326.24	267.41	24.08
Ag_2O-functionalized In_2O_3 nanowires	2	87.73	186.49	1.27
	6	132.04	236.55	1.36
	10	150.69	266.76	1.52

without Ag_2O functionalization. Accordingly, the change in conducting channel volume with flowing NO_2 gas, in the case of the functionalized sensor, is significantly smaller than that in the case of the unfunctionalized sensor. Since the amount of change in conducting channel volume is proportional to the amount of change in normal resistance, the sensor response or sensitivity, which is defined as $S = R_{NO2}/R_{air}$, of the functionalized sensor is expected to be smaller than that of the unfunctionalized sensor. This expectation agrees with Fig. 5 with respect to the sensor responses. In addition, by Ag_2O functionalization, the exposed effective area of the In_2O_3 surface is inevitably decreased, contributing to the reduction in sensitivity.

On the other hand, because of Ag_2O functionalization, response and recovery times are significantly reduced (Table I). There will be several reasons behind these observations. First, it is surmised that Ag_2O will act as a catalyst and reduce the activation energies for both adsorption and desorption of the surface species (i.e., NO_2). A previous study revealed that the activation energy for adsorption and desorption can be lowered by catalytic activation.[24] Second, the spillover effect of the Ag_2O nanoparticles will shorten the response time. In this case, the metallic oxide, Ag_2O, easily and effectively adsorbs and dissociates the NO_2 gas species. However, Ag_2O itself does not directly contribute to the enhancement of sensing behavior with respect to response and recovery times. The surface of the main sensor material, the In_2O_3 nanowire, in the present system does not provide efficient adsorption and dissociation sites for NO_2 gas. Accordingly, the NO_2 gas will be preferentially adsorbed and dissociated on the Ag_2O phase and will subsequently migrate to the In_2O_3 nanowire surface.

Similarly, Zalvidea et al. previously reported that Pd catalyst provided an efficient dissociation rate of H_2 and rapid diffusion of H atoms, improving the response time of hydrogen sensors.[40] Accordingly, more NO_2 molecules concentrate onto the narrower exposed In_2O_3 core surface, enhancing the number of impinging species per unit surface area and time. This explains the decrease in the response/recovery times of the sensor upon Ag_2O functionalization.

In addition, from the data in Table I, we estimate that the response time has been diminished by 74.6, 61.2, and 53.8%, at NO_2 concentrations of 2, 6, and 10 ppm, respectively. Also, the calculation reveals that the recovery time has been diminished by 34.9, 1.7, and 0.2%, at the NO_2 concentrations of 2, 6, and 10 ppm, respectively. Accordingly, in the case of catalytic activation, the activation for adsorption is more severely lowered than that for desorption. Furthermore, it is noteworthy that the catalytic activation is more efficient in shortening the response and recovery times at a lower concentration of NO_2 gas.

In a previous study on the ethanol sensing behavior of In_2O_3:Ag composite nanoparticle layers, the enhanced gas sensing response is associated with the transformation of a depletion layer at the Ag_2O–In_2O_3 interface to an accumulation layer in Ag–In_2O_3.[37] It is possible that the adsorption of ethanol gas generates the electron accumulation layer, significantly decreasing the resistivity. On the other hand, because of the adsorption of NO_2 gas, the conversion of Ag_2O to Ag is considerably limited. Accordingly, in the present case of using NO_2 gas, the enhancement of sensitivity owing to the appearance of the Ag phase will be negligible. However, as stated previously, the Ag_2O nanoparticles will enhance the sensing behavior with respect to response and recovery times as a result of the spillover effect.

4. Conclusions

We have fabricated Ag_2O-functionalized In_2O_3 nanowires via a two-step process. In the first step, the Ag layer was sputtered onto the In_2O_3 nanowires, TEM investigation revealed that nanoparticles with a cubic Ag phase were generated on the surface of the In_2O_3 nanowires. XRD and TEM investigations coincidentally revealed that the Ag shell layer was transformed into cubic-Ag_2O-phase nanoparticles by thermal heating in the 2nd step. SEM images revealed that the products consist of 1D nanostructures regardless of the shell-coating and subsequent annealing. We compared the NO_2 sensing characteristics among sensors fabricated from Ag_2O-functionalized nanowires and from bare In_2O_3 nanowires. The sensor response or sensitivity of the Ag_2O-functionalized sensor was considerably lower than that of the nonfunctionalized sensor, presumably because the Ag_2O functionalization effectively reduces the conduction channel volume of the initial stage without introducing NO_2 gas. Also, the Ag_2O functionalization greatly reduced the response and recovery times of In_2O_3 nanowire-based gas sensors. With Ag_2O functionalization, the catalytic effect and/or spillover effect of Ag_2O nanoparticles facilitates the concentrated flow of species onto the exposed In_2O_3 surface, shortening the response/recovery time.

Acknowledgement

This work was supported by the National Research Foundation of Korea (NRF) grant funded by the Korea government (MEST) (No. 2012029262).

1) G. Neri, A. Bonavita, G. Micali, G. Rizzo, N. Pinna, and M. Niederberger: Sens. Actuators B **127** (2007) 455.
2) G. Korotcenkov, A. Cerneavschi, V. Brinzari, A. Vasiliev, M. Ivanov, A. Cornet, J. Morante, A. Cabot, and J. Arbiol: Sens. Actuators B **99** (2004) 297.
3) M. Ivanovskaya, A. Gurlo, and P. Bogdanov: Sens. Actuators B **77** (2001) 264.
4) M. Ali, C. Y. Wang, C.-C. Röhlig, V. Cimalla, T. Stauden, and O. Ambacher: Sens. Actuators B **129** (2008) 467.
5) G. Korotcenkov, V. Brinzari, A. Cerneavschi, M. Ivanov, A. Cornet, J. Morante, A. Cabot, and J. Arbiol: Sens. Actuators B **98** (2004) 122.
6) W.-Y. Chung, G. Sakai, K. Shimanoe, N. Miura, D.-D. Lee, and N.

Yamazoe: Sens. Actuators B **46** (1998) 139.
7) P. S. Khiabani, A. Hosseinmardi, E. Marzbanrad, S. Ghashghaie, C. Zamani, M. Keyanpour-Rad, and B. Raissi: Sens. Actuators B **162** (2012) 102.
8) J. M. Lee, F. Xia, W. T. Nichols, C. Choi, and W. I. Park: Met. Mater. Int. **18** (2012) 875.
9) K. B. Lee, J. H. Seo, J. P. Ahn, H. Kwon, and H. R. Yang: Met. Mater. Int. **18** (2012) 727.
10) S. Kim, M. S. Kim, G. Nam, and J.-Y. Leem: Electron. Mater. Lett. **8** (2012) 445.
11) H. W. Kim, J. C. Yang, H. G. Na, D. S. Kwak, and C. Lee: Met. Mater. Int. **18** (2012) 705.
12) M.-Y. Kim, B.-K. Yu, and T.-S. Oh: Electron. Mater. Lett. **8** (2012) 269.
13) M.-S. Seo and H. Lee: Electron. Mater. Lett. **8** (2012) 259.
14) W. Lim, J. S. Wright, B. P. Gila, J. L. Johnson, A. Ural, T. Anderson, F. Ren, and S. J. Pearton: Appl. Phys. Lett. **93** (2008) 072109.
15) A. Vomiero, S. Bianchi, E. Comini, G. Faglia, M. Ferroni, N. Poli, and G. Sberveglieri: Thin Solid Films **515** (2007) 8356.
16) V. V. Sysoev, T. Schneider, J. Goschnick, I. Kiselev, W. Habicht, H. Hahn, E. Strelcov, and A. Kolmakov: Sens. Actuators B **139** (2009) 699.
17) D.-T. Phan and G.-S. Chung: Sens. Actuators B **161** (2012) 341.
18) S. S. Kim, J. Y. Park, S.-W. Choi, H. S. Kim, H. G. Na, J. C. Yang, and H. W. Kim: Nanotechnology **21** (2010) 415502.
19) S. S. Kim, J. Y. Park, S.-W. Choi, H. G. Na, J. C. Yang, and H. W. Kim: J. Alloys Compd. **509** (2011) 9171.
20) A. Chowdhuri, S. K. Singh, K. Sreenivas, and V. Gupta: Sens. Actuators B **145** (2010) 155.
21) J. Y. Shim, J. D. Lee, J. M. Jin, H. Cheong, and S.-H. Lee: Sol. Energy Mater. Sol. Cells **93** (2009) 2133.
22) T. Xu, H. Huang, W. Luan, Y. Qi, and S.-T. Tu: Sens. Actuators B **133** (2008) 70.
23) P. Bogdanov, M. Ivanovskaya, E. Comini, G. Faglia, and G. Sberveglieri: Sens. Actuators B **57** (1999) 153.
24) A. Helwig, G. Müller, G. Sberveglieri, and G. Faglia: Sens. Actuators B **126** (2007) 174.
25) G. Leo, R. Rella, P. Siciliano, S. Capone, J. C. Alonso, V. Pankov, and A. Ortiz: Sens. Actuators B **58** (1999) 370.
26) S. T. Shishiyanu, T. S. Shishiyanu, and O. I. Lupan: Sens. Actuators B **113** (2006) 468.
27) C. Cantalini, W. Wlodarski, H. T. Sun, M. Z. Atashbar, M. Passacantando, A. R. Phani, and S. Santucci: Thin Solid Films **350** (1999) 276.
28) C. Cantalini, W. Wlodarski, H. T. Sun, M. Z. Atashbar, M. Passacantando, and S. Santucci: Sens. Actuators B **65** (2000) 101.
29) C.-Y. Lin, Y.-Y. Fang, C.-W. Lin, J. J. Tunney, and K.-C. Ho: Sens. Actuators B **146** (2010) 28.
30) N. H. Kim and H. W. Kim: Appl. Surf. Sci. **242** (2005) 29.
31) H. W. Kim, S. H. Shim, J. W. Lee, J. Y. Park, and S. S. Kim: Chem. Phys. Lett. **456** (2008) 193.
32) S.-W. Choi, J. Y. Park, and S. S. Kim: Nanotechnology **20** (2009) 465603.
33) J. Y. Park, S.-W. Choi, J.-W. Lee, C. Lee, and S. S. Kim: J. Am. Ceram. Soc. **92** (2009) 2551.
34) J. Y. Park, S.-W. Choi, and S. S. Kim: Nanoscale Res. Lett. **5** (2010) 353.
35) H. W. Kim, S.-W. Choi, A. Katoch, and S. S. Kim: Sens. Actuators B **177** (2013) 654.
36) S. T. Shishiyanu, T. S. Shishiyanu, and O. I. Lupan: Sens. Actuators B **107** (2005) 379.
37) V. N. Singh, B. R. Mehta, R. K. Joshi, F. E. Kruis, and S. M. Shivaprasad: Sens. Actuators B **125** (2007) 482.
38) C. Bittencourt, E. Llobet, P. Ivanov, X. Vilanova, X. Correig, M. A. P. Silva, L. A. O. Nunes, and J. J. Pireaux: J. Phys. D **37** (2004) 3383.
39) V. N. Singh, B. R. Mehta, R. K. Joshi, and F. E. Kruis: J. Nanomater. **2007** (2007) 28031.
40) D. Zalvidea, A. Díez, J. L. Cruz, and M. V. Andrés: Sens. Actuators B **114** (2006) 268.